A Detailed Molecular Belt Model for Apolipoprotein AI in Discoidal High Density Lipoprotein

Article *in* Journal of Biological Chemistry · December 1999

DOI: 10.1074/jbc.274.45.31755 · Source: PubMed

Communication

THE JOURNAL OF BIOLOGICAL CHEMISTRY
Vol. 274, No. 45, Issue of November 5, pp. 31755–31758, 1999

A Detailed Molecular Belt Model for Apolipoprotein A-I in Discoidal High Density Lipoprotein*

(Received for publication, August 3, 1999, and in revised form, August 18, 1999)

Jere P. Segrest‡§¶‖, Martin K. Jones‡§, Anthony E. Klon¶, Christopher J. Sheldahl¶, Matthew Hellinger¶, Hans De Loof§, and Stephen C. Harvey¶

From the ‡Department of Medicine, the §Atherosclerosis Research Unit, and the ¶Department of Biochemistry and Molecular Genetics, University of Alabama Birmingham Medical Center, Birmingham, Alabama 35294

Apolipoprotein A-I (apoA-I) is the principal protein of high density lipoprotein particles (HDL). ApoA-I contains a globular N-terminal domain (residues 1–43) and a lipid-binding C-terminal domain (residues 44–243). Here we propose a detailed model for the smallest discoidal HDL, consisting of two apoA-I molecules wrapped beltwise around a small patch of bilayer containing 160 lipid molecules. The C-terminal domain of each monomer is ringlike, a curved, planar amphipathic α helix with an average of 3.67 residues per turn, and with the hydrophobic surface curved toward the lipids. We have explored all possible geometries for forming the dimer of stacked rings, subject to the hypothesis that the optimal geometry will maximize intermolecular salt bridge interactions. The resulting model is an antiparallel arrangement with an alignment matching that of the (nonplanar) crystal structure of lipid-free apoA-I.

Apolipoprotein (apo)[1] A-I is the major protein component of the antiatherogenic high density lipoproteins (HDL). There are eight 22-mer and two 11-mer tandem amino acid sequence repeats, each with the periodicity of an amphipathic α helix (1, 2), often punctuated by prolines, encoded in exon 4 of the apoA-I gene (residues 44–241).

ApoA-I is an integral component of both spheroidal circulating HDL particles and the geometrically simpler discoidal (hockey puck-like) nascent HDL particles. The better characterized discs are small unilamellar bilayers, containing approximately 160 molecules of phospholipid, surrounded by two apoA-I monomers (3–5). Two general models have been proposed for apoA-I on the disc rim: (i) two molecules of apoA-I form a pair of continuous amphipathic α helices parallel to the plane of the disc (the "double belt" model) (3, 6–8); (ii) the 22-mer amphipathic α helical repeats of apoA-I form tandem antiparallel helices perpendicular to the plane of the disc (the "picket-fence" model) (9, 10). Although total reflectance Fourier-transform infrared spectroscopy studies of discoidal HDL have been interpreted as supportive of the picket-fence model (11) because the samples were dried prior to study, these conclusions are open to question. A recent study of discoidal HDL using polarized internal reflection infrared spectroscopy under native conditions unambiguously supports the belt model (12).

In the recently published x-ray structure, residues 44–243 of apoA-I form an almost continuous amphipathic α helix, and the authors suggest that these results support the double belt model for discoidal HDL (7). Because lipid has a profound effect on the conformation and orientation of protein that interacts with it (13, 14), we hypothesized that if the double belt model was correct, the geometry of a planar bilayer disc should place constraints upon lipid-associated apoA-I such that the hydrophobic face of a continuous amphipathic α helix would: a) be confined to a plane and b) form the inside of a continuous amphipathic α helical torus.

EXPERIMENTAL PROCEDURES

Helical Net and Helical Wheel Programs—Previously published helical net (HELNET) and helical wheel (WHEEL) programs (15) were modified to create a PITCH = *x* option to allow unlimited variation of the 3.6 residue/turn pitch of an idealized α helix.

Determination of ϕψ Coordinates for a Model α11/3 Helical Ring—This was achieved by trial and error exploration of the ϕψ coordinates in the Ramachandran space of an α helix using TRIPOS SYBYL6.5 run on an SGI Elan 4000 workstation.

Program for Scoring of Salt Bridge—A modification of the HELNET program (15), ALIGN, was developed to sum a weighted score of salt bridges and charge appositions for each helix-helix docking position of the three possible interfacial orientations. Interfacial orientations were determined by the L lipid affinity algorithm (16, 17). Salt bridges and charge appositions were found by taking the helical net of helices 1–10 of one apoA-I α11/3 helix monomer and inverting and superimposing its L or R interface onto the L or R interface of a second monomer beginning with complete overlap between them. Interactions were eliminated by distance between residues down the helix axis, by radial distance between residues, and by radial distance of their average position from the polar-nonpolar interface. Salt bridges were assigned a negative score of −1 and like charge appositions a positive score of 1, weighted by a sliding scale reflecting the average position of their residue relative to the interface of the polar-nonpolar faces. The helical nets were translated relative to each other, one residue at a time, in a closed loop fashion as shown in Fig. 4*B*.

Building the Model HDL Particle—Two copies of the α helical ring described above were used to build the model dimer. The 10-Å distance between the α helix axes used in the model is typical of the center-to-center distance for α helices in protein crystal structures. Modest energy minimization was used to eliminate unacceptable steric clashes, using the QUANTA/CHARMM package (Molecular Simulations, Inc.). An 85-Å diameter discoidal lipid patch containing 161 POPC molecules was extracted from the simulation by Heller *et al.* (18) and docked into the protein ring. Some manual manipulation of individual lipid molecules was carried out to improve lipid/protein packing, again using QUANTA. Energy minimization of the entire protein/lipid complex converged in less than 5,000 cycles.

RESULTS

Amphipathic Helical Ring—Fig. 1*A* is a continuous α helical net display of tandem helices 1–10 of apoA-I plotted with the pitch of an idealized α helix, 3.6 (18/5) residues per turn; the hydrophobic face of helices 1–10 forms one complete turn of a

* This work was supported in part by National Institutes of Health Grant P01 HL-34343 (to J. P.S.). The costs of publication of this article were defrayed in part by the payment of page charges. This article must therefore be hereby marked "*advertisement*" in accordance with 18 U.S.C. Section 1734 solely to indicate this fact.

‖ To whom correspondence should be addressed. Tel.: 205-934-4420; Fax: 205-975-8079; E-mail: segrest@uab.edu.

[1] The abbreviations used are: apo, apolipoprotein; HDL, high density lipoprotein; POPC,1-palmitoyl-2-oleoyl-*sn*-glycero-3-phosphocholine.

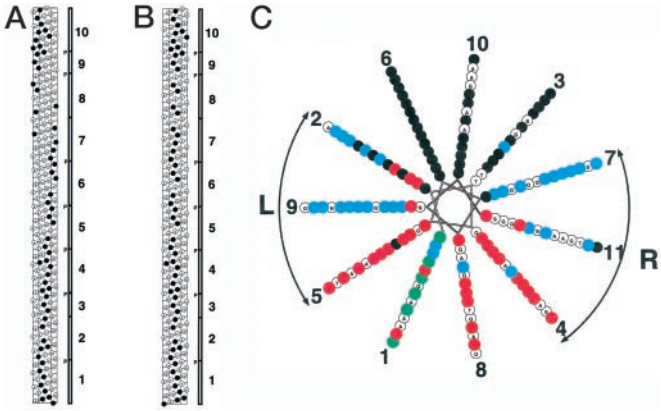

FIG. 1. **Helical net and helical wheel analyses of tandem amphipathic α helices 1–10 (residues 44–241) of human apoA-I.** Hydrophobic residues are indicated by *solid black circles*. Tandem helices and proline punctuations are indicated to the *right* of each net. *A*, helical net of tandem helices 1–10 of apoA-I plotted with an idealized pitch of 3.6 residues/turn using the HELNET program (15). *B*, helical net diagram of tandem helices 1–10 of apoA-I plotted with a pitch of 11/3 residues/turn using the HELNET program option (15), PITCH = 3.66667. *C*, helical wheel diagram, oriented with N-terminal up, of tandem helices 2–9 of apoA-I plotted with a pitch of 11/3 residues/turn using the WHEEL program option (15). Basic residues are represented by *solid blue circles*, acidic residues by *solid red circles*, and prolines by *solid green circles*. The left and right docking interfaces (see Figs. 2–4) are denoted by *arcs*.

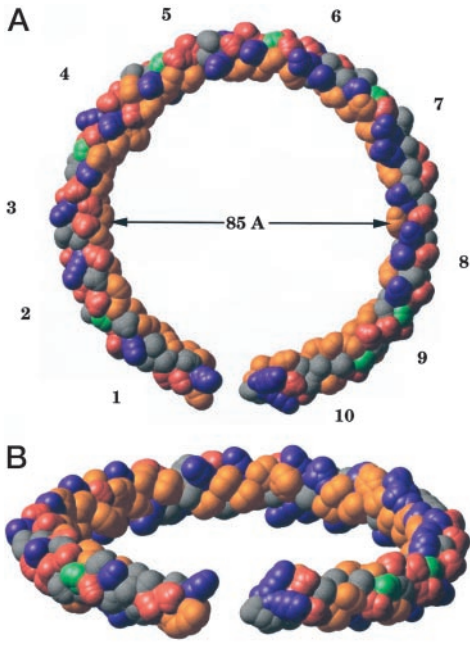

FIG. 2. **Space filling molecular graphics model of the 105-Å diameter α11/3 helical ring.** The figure is generated by RIBBONS (22). Hydrophobic residues are indicated in *orange*, prolines in *green*, basic residues in *blue*, acidic residues in *red*, and all other residues in *gray*. Tandem amphipathic α helices 1–10 are labeled. *A*, top view of the left interfacial surface (Fig. 1*C*) indicating inside diameter. *B*, side view.

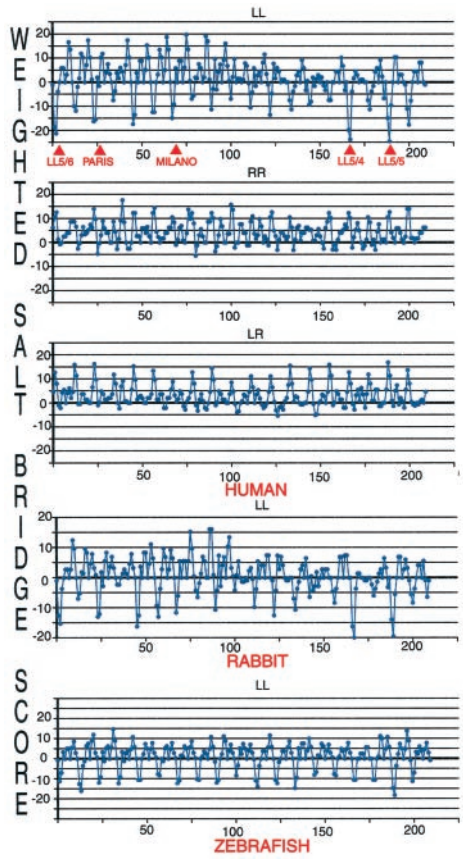

FIG. 3. **Weighted salt bridge scores of the three docking interfaces, LL, RR, and LR, determined using ALIGN.** A modification of the HELNET program (15), ALIGN, was used to score the weighted number of salt bridges and charge appositions for each docking position of three interfacial orientations of apoA-I, LL (antiparallel) for human, rabbit, and zebrafish, RR (antiparallel) for human, and LR (parallel) for human. For each residue step (*x* axis), representing one docking position, each weighted score is shown (*y* axis).

continuous right-handed spiral (pitch = 22/3.6 = approximately 6.11 residues per 22-mer repeat). If closed into a circle, this hydrophobic face would twist around the resulting torus, rather than lying on the inside as required for the belt model.

We then examined alternative possibilities. A continuous α helical net display of tandem repeats 1–10 plotted with a pitch of 3 turns per 11 residues (approximately 3.67 residues/turn), suggested by the 22-mer/11-mer tandem periodicity, creates a 198-residue α helix with a straight (planar) hydrophobic face (Fig. 1*B*). We call this an α11/3 helix, a structure essentially indistinguishable from an idealized α helix.[2]

Construction of a continuous α11/3 helical wheel diagram of tandem helices 2–9 of apoA-I is shown in Fig. 1*C*. Assigning the six prolines to helical wheel position 1, position 6 is occupied entirely, and positions 10 and 3 mostly, by hydrophobic residues, positions 9 and 7 mostly by positively charged residues, and positions 5, 8, and 4 mostly by negatively charged residues (the class A amphipathic α helix pattern (19). Only helical wheel position 2 is equally divided between positively and negatively charged residues, a result whose relevance will become apparent later.

Because of the increasing strength of hydrogen bonds in environments with decreasing dielectric constants, α helices have been shown to curve away from environments with higher, and toward those with lower, dielectric constants (20, 21). Dielectric gradient-induced helix curvature provided the solution to the problem of wrapping a continuous amphipathic α helix, hydrophobic face inward, around the edge of a lipid bilayer disc.

We next determined that $\phi = -58.7°$, $\psi = -48.8°$ produced an α11/3 helix. We then determined that $\phi = -55.8°$, $\psi = -45.9°$ for the hydrophobic residues at amphipathic α11/3 helical wheel positions 6, 10, 3, and 7 and $\phi = -61.6°$, $\psi = -51.7°$ for the polar residues at α11/3 helical wheel positions 8, 1

[2] A. E. Klon, J. P. Segrest, and S. C. Harvey, unpublished observation.

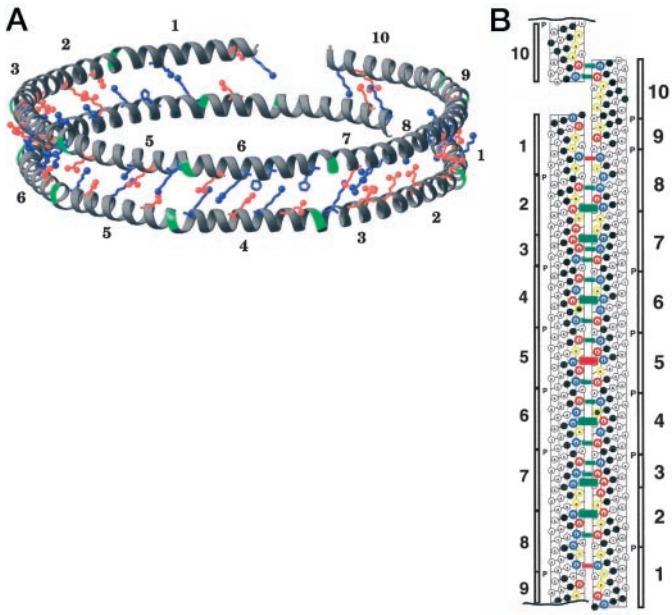

FIG. 4. **Structure and interhelical salt bridges of the LL5/5 model.** *A*, RIBBONS molecular graphics model (22) of the LL5/5 model. Tandem helices 1–10 are labeled. Only the charged residues (in extended conformation) at α11/3 helical wheel positions 2, 5, and 9 (Fig. 1*C*) are explicitly displayed; color coding is as in Fig. 1*C*. *B*, helical net diagram of the LL5/5 position for the α11/3 helical representation of tandem helices 1–10 of apoA-I plotted using the HELNET program options (15) REVERSE (to produce the antiparallel orientations) and PITCH = 3.66667. Residues in the 2, 5, and 9 positions are marked by *colored circles*; hydrophobic residues in other positions are represented by *solid black circles*. Interhelical interactions between α11/3 helical wheel positions 2–2 and 5–9 are indicated: salt bridges by *green dashes*, *broad* and *narrow*, respectively; interhelical like-charged appositions by *red dashes*, *broad* and *narrow*, respectively.

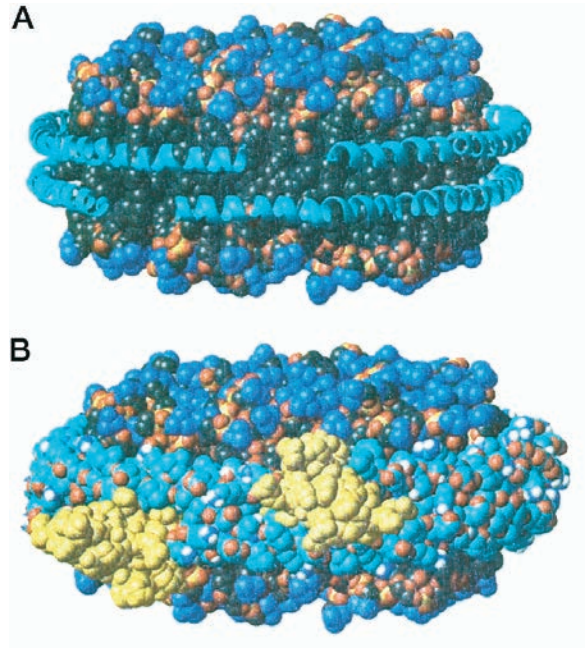

FIG. 5. **Space filling model of the LL5/5 model docked around the edge of an 85-Å diameter patch of molecular dynamics-simulated POPC bilayer in the liquid crystalline phase.** Color code for the 161 POPC molecules: $C(NH_2)_3$, *blue*; oxygen atoms, *red*; phosphorous atoms, *yellow*; all other atoms, *black*. *A*, docked LL5/5 model, displayed as a helical ribbon, oriented to show the gap regions between residue 44 of helix 1 and residue 241 of helix 10. *B*, docked LL5/5 model, displayed as an all-atom model, oriented as in *panel A*. To the gap region of each helical ring, a compact 43-residue protein domain (43-residue edited version of the PDB file of bovine pancreatic trypsin inhibitor, *gold*) has been added to represent residues 1–43 of intact apoA-I; the structure of this region of apoA-I is not known, but its deletion has no measurable effect on lipid association (24). Color code for apoA-I: nitrogen atoms, *blue*; oxygens atoms, *red*; carbon atoms, *cyan*; polar hydrogen atoms, *white*. Coordinates for this structure can be downloaded over the WWW at University of Alabama.

(exclusive of the prolines), and 5 (Fig. 1*C*) produced a planar amphipathic α helical torus, 80–85 Å inside diameter, 100–105 Å outside diameter, with a continuous, concave inner hydrophobic face (Fig. 2). We call this an α11/3 helical ring. Mapping of helix curvature onto an α11/3 helical model of residues 44–241 of apoA-I by systematic variation of $\phi\psi$ along the plane of curvature was a convenient surrogate for curvature induced by a dielectric gradient.

Helical Ring Dimer—We then examined possible interactions between two α11/3 helical rings by docking along, and rotating around, the axis of one ring relative to a second. Helical wheel positions 5, 9, and 2, and positions 7, 11, and 4, were designated the left and right docking interfaces, respectively, for the α11/3 helical rings (Fig. 1*C*). The two possible antiparallel ring pair interfaces, left to left (LL) and right to right (RR), and the single possible parallel ring pair interface, left to right (LR) were systematically rotated one residue at a time, and ring pair interactions were examined. A modification of the HELNET program (15), ALIGN, was used to score the weighted number of salt bridges and charge appositions for all orientations of the three ring pair interfaces (Fig. 3). Although there is some degree of 11-mer/22-mer periodicity in the rotational analyses of all three ring pair interfaces, there is a striking 11-mer periodicity in the minima of the LL ring pair, and all nineteen have a lower weighted salt bridge score than any of the RR or LR orientations (Fig. 3). For clarity, we defined a terminology that denotes the helix-helix stagger and interface in terms of 22 tandem repeats; *e.g.* LL5/5 refers to a position in which helix 5 in monomer-1 is associated with helix 5 in the monomer-2 along an LL antiparallel interface. Using this terminology, the three most impressive orientations of the LL ring pair have rank order weighted salt bridge scores of LL5/5 < LL5/4 < LL5/6 (Fig. 3).

It is worthy of note that the LL orientation with the lowest score, LL5/5, has the identical rotational stagger and interfacial orientation of the published x-ray structure (7). Fig. 4*A* is an angled view of a RIBBONS (22) representation of the LL5/5 model built with all-atom detail. In this model, only the charged residues (in extended conformation) at α11/3 helical wheel positions 5, 9, and 2 (Fig. 1*C*) are displayed. Note the almost perfect alignment of interhelix salt bridge pairs. In the LL5/5 model, of 20 interhelix salt bridges, 18 are between pairwise interactions of helices 5/5, 4/6, 3/7, and 2/8. In addition, helix 10 of monomer-1 and helix 10 of monomer-2 form an antiparallel overlap, identical to that in the x-ray structure (7), to create two additional interhelical salt bridges.

Interhelix salt bridges for the LL5/5 model are denoted more clearly by an α11/3 helical net diagram (Fig. 4*B*). Of the 20 interhelix salt bridges formed, six are between α11/3 helical wheel positions 2–2, and fourteen are between α11/3 helical wheel positions 5–9 and 9–5. Note the absence of interhelical salt bridges between the middle of helix 8 and the C-terminal half of helix 1, between helix 9 and the N-terminal half of helix 1, and between the N-terminal two-thirds of helix 10 and the helix 1–10 gap; the C-terminal half of helix 1 and the N-terminal half of helix 10 are nonhelical in the x-ray structure (7).

Molecular Belt Model for Discoidal HDL—Fig. 5 is a space filling model of the LL5/5 α11/3 helical ring dimer docked around the edge of an 85-Å diameter patch of molecular dynamics-simulated POPC bilayer (18) containing 161 POPC

molecules. This model of a POPC:apoA-I discoidal HDL particle is in excellent agreement with the observed dimensions (100–105-Å diameter) and composition (2 apoA-I and 160 POPC molecules) of the particle (5). The two gold-colored globules placed in the gap regions in Fig. 5*B* are globular protein fragments extracted from the Protein Data Bank; the sole purpose for pasting these fragments on the model is to indicate the relative size of residues 1–43 of apoA-I (structure unknown) to the model.

Discoidal HDL particles containing three apoA-I monomers have been reported (23). The LL5/5 model can accommodate a third apoA-I molecule folded in the middle of helix 5 as an apoA-I helical hairpin (7, 24).

Tests of the Plausibility of the Model—Two tests of the plausibility of the double belt model were made. First, natural mutations in human apoA-I, many associated with low HDL (23), were analyzed; two results are worthy of note. (i) Point mutations in human apoA-I (23) are highly asymmetrically distributed when superimposed upon the α11/3 helical wheel of helices 2–9; of the 25 point mutations of human apoA-I reported in the literature, 12 are located at positions 5, 9, and 2 (L docking interface) and only 1 at positions 7, 11, and 4 (R docking interface). The picket-fence model for discoidal HDL that should involve alternating LL and RR antiparallel salt bridges would seem unlikely to produce this degree of asymmetry. (ii) Disulfide-linked homodimers of apoA-I have been isolated from two mutations of human apoA-I (R173C and R151C) (23). Both mutations are at position 9 on the L docking interface, the interface in the LL model that is in contact with itself; LL self-contact between identical helices from two apoA-I monomers seems unlikely to be allowed in a picket-fence model. All atom modeling demonstrates that position 9, because it lies precisely on the left interfacial packing edge, is the only radial position in the LL model at which van der Waals contacts between identical helices from two apoA-I monomers would allow formation of a homodimer disulfide bond.[2] Both mutant homodimers would fix the rotation of the ring dimer at positions other than the LL5/5 orientation (interestingly at local salt bridge minima, Fig. 3), and both result in diminished circulating HDL levels.

As a second test, we examined the phylogenetic conservation of apoA-I. While individual salt bridges are often, but not always, conserved, the general ALIGN pattern, in which multiple orientations of the LL ring pair display lower weighted salt bridge scores than any of the RR or LR orientations, holds for all species examined: mammals, birds, and fish; ALIGN plots for the LL orientation for rabbit and zebrafish are shown in Fig. 3.

DISCUSSION

The salt bridge pattern of the LL5/5 model is encoded into the 11-mer tandem sequence repeats of apoA-I, reflecting the geometric relationship of the α11/3 helix to the conformation of apoA-I on the edge of discoidal HDL. A remarkable feature of this detailed molecular model for disc-associated apoA-I is the almost perfect interhelical alignment of charged side chains in the 2–2 and 5–9 paired positions.

The LL5/5 model for lipid-associated apoA-I was derived entirely from three simple conformational constraints, (i) the amphipathic α helix as the major lipid-associating motif of apoA-I (1, 2, 13, 16), (ii) planar discoidal HDL geometry (3–5, 9), and (iii) curvature dictated by the boundary between the low dielectric lipid and the high dielectric solvent (20, 21), each of which is supported by abundant experimental evidence. Because of its prediction of specific salt bridges, the LL5/5 model, unlike the picket-fence model, is eminently testable by site-directed mutagenesis. To the extent that lipid-water interfaces inscribe a "signature" in lipid-associating proteins, the detailed molecular model for discoidal HDL developed here implies that atomic resolution models for other lipoproteins may be achievable by the systematic application of the principle of the "lipid signature."

Acknowledgments—We thank Drs. David Borhani, Christie Brouillette, G. M. Anantharamaiah, Vinod Mishra, and Jeffery Engler for helpful discussions.

REFERENCES

1. Segrest, J. P., Jackson, R. L., Morrisett, J. D. & Gotto, A. M., Jr. (1974) *FEBS Lett.* **38,** 247–253
2. Fitch, W. M. (1977) *Genetics* **86,** 623–644
3. Wlodawer, A., Segrest, J. P., Chung, B. H., Chiovetti, R., Jr. & Weinstein, J. N. (1979) *FEBS Lett.* **104,** 231–235
4. Atkinson, D., Small, D. M. & Shipley, G. G. (1980) *Ann. N. Y. Acad. Sci.* **348,** 284–298
5. Jonas, A., Wald, J. H., Toohill, K. L., Krul, E. S. & Kezdy, K. E. (1990) *J. Biol. Chem.* **265,** 22123–22129
6. Segrest, J. P. (1977) *Chem. Phys. Lipids* **18,** 7–22
7. Borhani, D. W., Rogers, D. P., Engler, J. A. & Brouillette, C. G. (1997) *Proc. Natl. Acad. Sci. U. S. A.* **94,** 12291–12296
8. Rogers, D. P., Roberts, L. M., Lebowitz, J., Datta, G., Anantharamaiah, G. M., Engler, J. A. & Brouillette, C. G. (1998) *Biochemistry* **37,** 11714–11725
9. Tall, A. R., Small, D. M., Deckelbaum, R. J. & Shipley, G. G. (1977) *J. Biol. Chem.* **252,** 4701–4711
10. Nolte, R. T. & Atkinson, D. (1992) *Biophys. J.* **63,** 1221–1239
11. Wald, J. H., Coormaghtigh, E., De Meutter, J., Ruysschaert, J. M. & Jonas, A. (1990) *J. Biol. Chem.***265,** 20044–20050
12. Koppaka, V., Silvestro, L., Engler, J. A., Brouillette, C. G. & Axelsen, P. H. (1999) *J. Biol. Chem.* **274,** 14541–14544
13. Segrest, J. P., Jones, M. K., De Loof, H., Brouillette, C. G., Venkatachalapathi, Y. V. & Anantharamaiah, G. M. (1992) *J. Lipid Res.* **33,** 141–166
14. Richardson, J. S. & Richardson, D. C. (1989) *Principles and Patterns of Protein Conformation*, pp. 1–98, Plenum Press, New York
15. Jones, M. K., Anantharamaiah, G. M. & Segrest, J. P. (1992) *J. Lipid Res.* **33,** 287–296
16. Palgunachari, M. N., Mishra, V. K., Lund-Katz, S., Phillips, M. C., Adeyeye, S. O., Alluri, S., Anantharamaiah, G. M. & Segrest, J. P. (1996) *Arterioscler. Thromb. Vasc. Biol.* **16,** 328–338
17. Mishra, V. K. & Palgunachari, M. N. (1996) *Biochemistry* **35,** 11210–11220
18. Heller, H., Schaefer, M. & Schulten, K. (1993) *J. Phys. Chem.* **97,** 8343–8360
19. Segrest, J. P., De Loof, H., Dohlman, J. G., Brouillette, C. G. & Anantharamaiah, G. M. (1990) *Proteins* **8,** 103–117
20. Blundell, T., Barlow, D., Borkakoti, N. & Thornton, J. (1983) *Nature* **306,** 281–283
21. Zhou, N. E., Zhu, B. Y., Sykes, B. D. & Hodges, R. S. (1992) *J. Am. Chem. Soc.* **114,** 4320–4326
22. Carson, M. (1991) *J. Appl. Crystallogr.* **24,** 958–961
23. Brouillette, C. G. & Anantharamaiah, G. M. (1995) *Biochim. Biophys. Acta* **1256,** 103–129
24. Rogers, D. P., Brouillette, C. G., Engler, J. A., Tendian, S. W., Roberts, L., Mishra, V. K., Anantharamaiah, G. M., Lund-Katz, S., Phillips, M. C. & Ray, M. J. (1997) *Biochemistry* **36,** 288–300

COMMUNICATION:

A Detailed Molecular Belt Model for Apolipoprotein A-I in Discoidal High Density Lipoprotein

Jere P. Segrest, Martin K. Jones, Anthony E. Klon, Christopher J. Sheldahl, Matthew Hellinger, Hans De Loof and Stephen C. Harvey

J. Biol. Chem. 1999, 274:31755-31758.
doi: 10.1074/jbc.274.45.31755